

On the Mapping Efficiency of Integral Field vs Longslit Spectrographs: Comparison of the UIST/IFU and CGS4 at UKIRT using Uranus in the K–L Bands

L. M. Trafton

McDonald OBServatory and Department of Astronomy
University of Texas at Austin, Austin TX 78712
lmt@astro.as.utexas.edu

T. R. Geballe

Gemini Observatory 670 N. A'ohoku Place, Hilo HI 96720

S. Miller

Department of Physics and Astronomy
University College London
Gower Street, London, WC1 6BT, England, UK

T. Stallard

Department of Physics and Astronomy
University College London
Gower Street, London, WC1 6BT, England, UK

Abstract

Although spectra of small extended objects are often more efficiently mapped using a spectrograph equipped with an integral field unit (IFU) than by sequential observations with one using a long slit, this is not always the case. We compared the efficiency of the United Kingdom Infrared Telescope (UKIRT) Imaging Spectrograph (UIST) with the Integral Field Unit attached vs the UKIRT Cassegrain longslit spectrograph CGS4 using low-dispersion observations of Uranus in the K, L, and L' bands. Uranus is a good test object because the size of its disk is comparable to the dimensions of the IFU aperture and it exhibits both a continuum and emission lines. Accounting for differences in spectral and spatial resolution, exposure time, sampling, and the IFU aperture width vs CGS4 slit width, we found that in spite of the IFU capability to obtain spatially resolved spectra over most of its aperture simultaneously, Uranus' disk is more efficiently mapped with CGS4 by using multiple longslit exposures. The decision as to which type of instrument is better for observing a particular extended object has to consider the both the object's and instrument's properties in detail.

1 Introduction

The coupling of an Integral Field Unit (IFU) to an astronomical spectrograph allows a spectrum for each pixel of sky in the IFU field to be obtained simultaneously. Not only is this capability useful for investigating an increasing number of interesting astronomical objects having spatial structure, but also it may provide the most efficient way to map a field spectrally. A spectrograph so equipped can spectrally map its 2-D field in a single exposure, obviating the need for multiple sequential spectrographic observations. With adequate throughput, such an instrument would normally be the spectrograph of choice at astronomical observatories for observing moderately extended objects.

However, spectrally mapping an extended object using a spectrograph equipped with an IFU unit is not always more efficient than sequential mapping with the spectrograph

alone. An example of such a case is a large object for which the spatial structure varies only slightly over the dimensions of the IFU field. In this case, multiple IFU exposures are needed for useful mapping, which might be done with greater sensitivity with multiple longslit exposures. Moreover, if the extended source is too large to be noddled along the relatively short IFU aperture, compared to a spectrographic longslit, there is a 50% loss of efficiency from having to nod the telescope between object and sky. The addition of the IFU unit necessarily reduces the throughput of the spectrograph owing to multiple beam reflections needed to slice the image into a stacked spectrum. A given signal will therefore yield a lower S/N ratio which, at sufficiently faint signal levels, will negate the IFU advantage relative to multiple exposures with a longslit spectrograph that covers the same field.

This paper compares the performance of the UIST/IFU imaging spectrograph (Ramsay et al. 2000; Todd et al. 2003) vs the CSG4 Cassegrain longslit spectrograph (0."61 wide slit) (Mountain et al. 1990) at the United Kingdom Infrared Telescope (UKIRT) telescope. The comparison is based on observations of Uranus at low dispersion by both instruments in the K-band continuum and K-, L-, and L'-band emission lines of H₂ and H₃⁺. Uranus is a good test object because its angular diameter is comparable to the 3."3 IFU aperture width and it exhibits both continuum and emission line spectra. The observing efficiency for the individual spectral bands is compared separately (rather than for the entire wavelength region from the beginning of the K-band through the L'-band). Despite the relative ease of using the IFU, this is one case where the relatively low throughput of the IFU favors multiple exposures with a longslit spectrograph. We conclude that the decision whether to use an imaging vs longslit spectrograph to map a particular extended astronomical object has to consider the pertinent details of the object in question; i.e., its brightness, spatial structure, size, rotation rate, and possibly the relative brightness of emission lines vs continuum.

2 Observations

In the K band, CH₄ lines and pressure-induced transitions of H₂ strongly absorb the incident solar near-IR continuum in Uranus' atmosphere. A deep haze layer produced by tropospheric CH₄ condensation and stratospheric photochemistry then diffusively reflects the sunlight, which is further absorbed along its exit path by CH₄ and H₂ above the reflecting haze particles (Fink and Larson 1979; Baines et al. 1995; Trafton et al. 1999). Superimposed on the resulting disk continuum are spectrally unresolved, hot, thermospheric line emission from the fundamental H₂ quadrupole spectrum. Disk-wide emission in the spectrally unresolved fundamental-band lines of H₃⁺ originating in Uranus' hot ionosphere are resolved from each other in the L- and L'-band windows (Lam et al. 1997; Trafton et al. 1993; 1999). The continuum in the L-L' bands is too weak for detection owing to strong planetary CH₄ absorption.

To accommodate making the comparison at similar spectral resolutions in each wavelength band, we use CGS4 spectra obtained along Uranus' diameter in conjunction with UIST/IFU spectra obtained with the HK, Short L, and Long L grisms (R=800–2300). The CGS4 observations were obtained by the authors at the UKIRT telescope in June 2001. During these observations, Uranus was noddled between two positions along the slit, which was one pixel wide. The spectrographic configuration employed was the frequently-used 40 l/mm grating (in 1st order) and the 300 mm "long" camera. The spectral resolution was $R=400*\lambda$, where λ is the wavelength in μm . The array was translated a distance of 1 2/3 pixels over 6 equal steps. Thus, the merged spectrum was sampled every 1/3 pixel. Uranus' diameter at the time was 3."63 and its position angle was 259°. The slit was oriented across the equatorial diameter and the sub-Earth latitude was -24°. The extracted spectra average the 7 brightest rows (pixels 0."61 along slit), which excludes the rings given the 0."7 seeing. Separate observations were obtained for the K-band and for the combined L-bands (L and L' combined in a single spectrum). During the 1.3 hr exposure, the planet rotated

27°, approximately equal to the width of 1.4 pixels at the center of Uranus’ disk. These observations are summarized in Table 1 along with the spectrographic parameters.

The UIST/IFU observing program on Uranus was carried out by UKIRT personnel during service “queue” observations during clear skies with moderately good seeing in Sep and Dec 2003 (see Table 1). The telescope was nodded between the object and sky. K-band spectra were obtained on Sep 10, 2003 and Dec 24, 2003. Short-L (L-band) spectra were obtained on Sep 22, 2003 and Long-L (L’-band) on Dec 23 and 24, 2003. During the September observations, Uranus’ apparent diameter varied over 3.”70→3.”68, and for December it was 3.”43. These compare with an effective rectangular IFU field of 3.”33 x 6.”43 on the sky. This field has 14 usable image slice columns (slitlets) each 0.”24 wide (two pixels) spanning the width of the effective aperture. Each pixel row is 0.”12 high. In September, Uranus’ diameter slightly overfilled the IFU aperture width; 83% of the planet would have been visible through the aperture with perfect seeing, or 10.3 square arcsec. For the post-quadrature December observations, 97% of Uranus would have been visible through the aperture with ideal seeing, or 8.91 square arcsecs. Note that 5.5 (operationally six with good seeing) CGS4 observations are needed to cover the single-exposure IFU field.

The dispersing was done by grisms located in the UIST; separate grisms with different dispersions were used for the different atmospheric windows. The HK grism, covering the H- and K-band windows, was helpful in acquiring Uranus into the IFU field. In the K-band and L-band, the effective spectral resolution was comparable to that of CGS4, but in the L’ window it was significantly higher.

TABLE 1
Observations

| Date (UT) | Mid-Obs (hr:min) | Exp Time (sec) | Observation (min) | Band | R | Slit Orientation (deg) |
|--------------|---------------------|-------------------------------|--------------------------|------|------|---------------------------|
| | | <u>(CGS4)^a</u> | <u>(0.”61 wide slit)</u> | | | |
| 2001 Jun 19 | 14:36 | 20 | 78 | L,L’ | 1500 | CM |
| 2001 Jun 19 | 12:32 | 30 | 70 | K | 840 | CM |
| | | <u>(UIST/IFU)^b</u> | <u>(0.”24 slices)</u> | | | |
| 2003 Sep 10 | 11:13 | 120 | 36 | K | 900 | ~EQ ^c |
| 2003 Sep 22 | 06:00 | 60 | 110 | L | 1380 | ” |
| 2003 Dec 23 | 04:07 | 20 | 71 | L’ | 2300 | ” |
| 2003 Dec 24 | 04:42 | 120 | 11 | K | 900 | ” |
| 2003 Dec 24 | 04:54 | 20 | 38 | L’ | 2300 | ” |

Uranus was nodded along the slit for CGS4 observations only. CM=central meridian; EQ= Equator.

^a40 l/mm grating, 1st order, 300 mm camera, and 0.”61 x 0.”61 sky pixels (the most commonly available configuration)

^bHK, Short-L, & Long-L grisms with 0.”24 x 0.”12 sky pixels

^cThe IFU long dimension was oriented NS or nearly in Uranus’ equatorial plane (Uranus PA=258°).

For all of our UIST/IFU observations of Uranus, the long dimension of the aperture (i.e., the image slices) was oriented north-south on the sky. The position angle of Uranus’ north (IAU) pole was 258°. This is the hidden pole; the visible south pole (i.e. the right-hand-rule

north pole) had position angle 78° so that the south end of the IFU image in the aperture was the sunrise limb of the planet. The image slices were therefore nearly aligned with Uranus' equatorial diameter. With a sub-earth latitude of -18° , less than 3% of Uranus' foreground disk was occulted by rings.

3 Reduction

The data were all flux-calibrated and converted to intensity per pixel in units $\text{W m}^{-2} \mu\text{m}^{-1} \text{sr}^{-1}$. The CGS4 data were reduced in 2001 by standard longslit methods. A single 1-D flux spectrum was extracted from Uranus' spectral image by summing the 7 brightest spectral rows ($4.''27$) across the disk diameter, which excluded light from the rings. The result was divided by the solid angle defined by the slit width and planet diameter (unadjusted for $0.''7$ seeing) to derive the disk-averaged intensity spectrum. CGS4 covered most of the combined L- and L'-bands in a single spectrum. The final reduction step smoothed each CGS4 spectrum with a Gaussian having $\text{FWHM}=1.5$ pixels. The effect of this on the spectral resolution was a noticeable but marginal broadening of the emission lines because the CGS4 spectrum was sampled every $1/3$ pixel. For consistency, the reduced UIST/IFU spectra were also smoothed by 1.5 pixels. The resulting CGS4 spectra are shown in Figs. 1, 2, and 3 for the K-band, L-band, and L'-band, respectively. These are the longslit spectra against which the UIST/IFU observations were indirectly compared.

The corresponding UIST/IFU spectra are shown plotted below the offset CGS4 spectra. The pipeline reduction and associated flux calibration were adopted for the Short L and Long L spectra. Noise spikes from the many "cosmic ray" hits over the long exposures were largely removed by taking the median of the 14 data planes of dimension 54×1024 spanning dimensions along the IFU aperture slices and wavelength, respectively. This works well because Uranus' disk overfills the IFU aperture width, leading to a more rectangular Uranus section. The spectra were also line-cleaned before taking this median and the results compared with simply taking the median. They were found to be mostly in close agreement. We converted the IFU fluxes to specific intensity by dividing the flux per pixel by the solid angle of a pixel row in a single IFU image slice; i.e., the area of two $0.''12$ square pixels.

The S(0) and S(1) quadrupole emission lines of H_2 stand out clearly in the CGS4 K-band spectrum (Fig. 1) against the broad pressure-induced absorption band of H_2 forming the deep local continuum. Prominent emission lines from the H_3^+ R branch are seen in Fig. 2, which shows opposite ends of spectra taken by each instrument along with a telluric CH_4 absorption spectrum obtained from an A0 V star (BS 8518) with UIST/IFU. The whole CGS4 L-L' band spectrum is shown in Fig. 3, which includes the prominent fundamental-band Q branch lines of H_3^+ .

Uranus' image was located in the IFU aperture by partially summing the $14 \times 54 \times 1024$ data cube over wavelengths and displaying the resulting aperture field. An average 1-D intensity spectrum was extracted from the 54×1024 median spectral image by averaging, for each wavelength sampled, the intensity over a rectangular area defined by the rows spanning Uranus' image, and correcting the result for sky background. This was done by dividing by the ratio of the area of Uranus' disk that would not be occulted by the IFU aperture during ideal seeing to the area of the extraction rectangle. These areas were reported for the two observing runs in Section 2. The L'-band spectra from the two nights were merged into a single L'-band spectrum, weighted by exposure time.

Parts of the pipeline-reduced UIST/IFU HK and Long L (but not Short L) extracted 1-D spectra were negative owing to excessive sky background subtraction. As a result, the night sky OH line emission spectrum in the K-band was incompletely cancelled and the true continuum intensity uncertain. Not enough background sky was available in the IFU aperture for subtracting the uncancelled OH spectrum without adding unacceptable noise. We therefore differenced the nodded sky spectra at disparate airmasses to obtain a

suitable residual OH spectrum with the dark subtracted. This was scaled and subtracted from Uranus' HK spectrum to remove the residual OH line spectrum satisfactorily. This procedure was not needed at Long L because the sky emission cancelled much better.

To correct the negativity of HK, we offset its intensity spectrum by an amount proportional to the reciprocal of the standard star spectrum with the proportionality constant determined by the cancellation of the telluric water and CO₂ absorption bands. The result (Fig. 1) compares well with the CGS4 spectrum except for artifacts at 2.20 and 2.30 μm , presumably from cosmic ray hits that survived line cleaning.

Since the L and L' continua were too weak for detection, they delineated the varying zero-intensity level between the planetary emission lines. The extraction of the Long L emission line spectrum therefore entailed the subtraction of this background, which we effected by using a high-order polynomial.

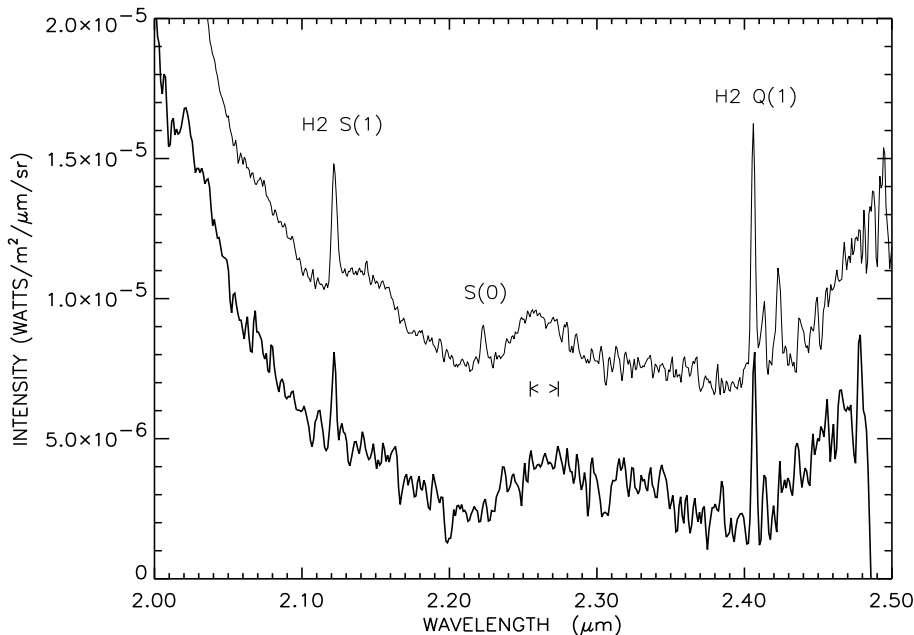


Fig. 1: Comparison of the extracted UIST/IFU spectrum of Uranus in the K-band obtained on 10 Sep 03 (heavy) (averaged over the portion of the disk in the IFU field) with a CGS4 spectrum extracted from Uranus' equatorial diameter obtained on 19 June 2001 (light, offset $+5 \times 10^{-6}$) at comparable resolution. Both spectra were smoothed during reduction by a Gaussian of FWHM=1.5 pixels and their exposure times are different. The IFU spectrum exhibits deep artifacts at 2.20 and 2.30 μm that survived line cleaning. The H₂ quadrupole S(1) and Q(1) lines are detected in both spectra; but the S(0) line (at 2.223 μm) and the Q(3) line are detected only with CGS4. The region marked at a relatively flat section of the continuum indicates the wavelength interval over which the standard deviations were sampled.

The data file headers incorrectly list the spectral resolution of the UIST/IFU as $R=2272$ for the Short-L grism and $R=3143$ for Long-L one at the effective band wavelengths. These design resolutions are degraded (presumably by the grism rulings; C. Davis, personal communication) as was determined by fitting Gaussian profiles to arc profiles as described on the UKIRT web site. The FWHM of the narrower lines of the telluric CH₄ absorption spectrum shown in Fig. 2 is consistent with the effective spectral resolution $R=1300$ obtained from the arc measurements (because the star image also fills an IFU slice during 0."7 seeing). As a result, the pixel sampling per effective spectral resolution element is greater than the two pixels that span the width of the IFU image slices; i.e. 3.6 pixels for Short L and 2.8 pixels for Long L.

The FITS header parameters for the wavelength scale and offset for the Short-L and Long-L IFU observations were found to be incorrect (as noted on the UIST web page). This is because they were determined from 2nd/3rd order arc spectra with blocking filters and our spectra were obtained in the 1st order, without those filters. The offset errors have been corrected in plotting Figs. 1–3.

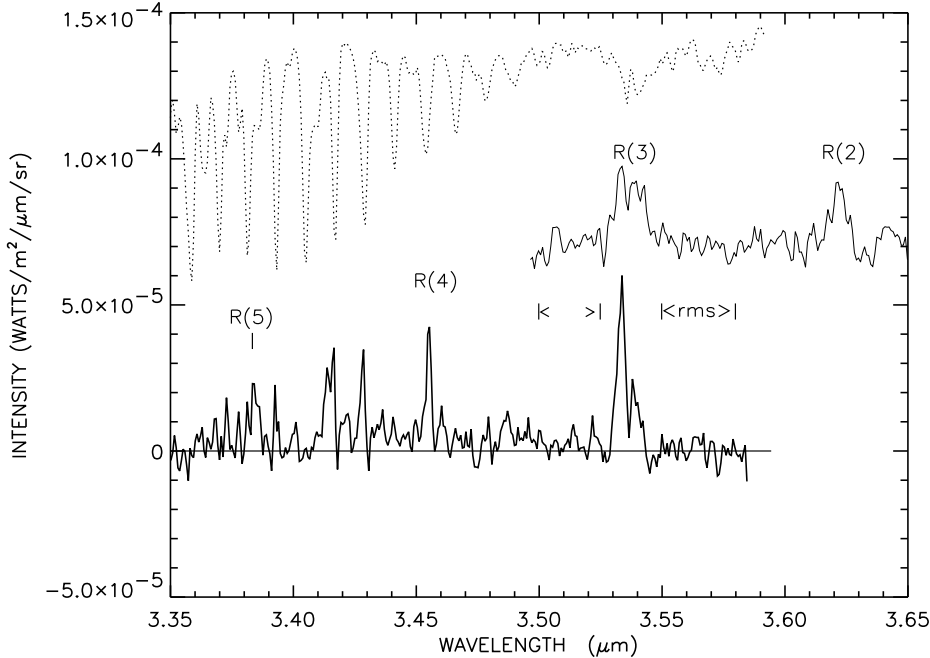


Fig. 2: Comparison of the extracted UIST/IFU spectrum of Uranus in the L band obtained on 22 Sep 2003 (heavy) (averaged over the portion of the disk visible in the IFU field) with a spectrum extracted from Uranus’ equatorial diameter obtained with CGS4 on 19 Jun 2001 (light; offset $+7 \times 10^{-5}$) at comparable resolution. The spectra overlap at the H_3^+ R(3) feature, which is distorted by telluric methane at critical Doppler shifts. All of the prominent features are from H_3^+ emission. The dotted spectrum at the top is that of a bright A0 V star (BS 8518) obtained with UIST/IFU showing the telluric methane absorption for comparison. All spectra have been smoothed by a Gaussian of FWHM=1.5 pixels. The ranges over which the standard deviation was sampled for the L-band continuum are marked.

4 Analysis

Our basic approach in comparing the efficiencies of these two instruments was to determine which instrument would take less time to map Uranus’ disk at useful S/N per common spectral and spatial resolution element (res. el.). Because the strength of either Uranus’ emission lines or continuum might have changed between the two sets of observations, it is better to compare the noise-equivalent intensity (NEI) of Uranus’ spectrum for the two instruments, rather than the S/N ratio. Defining the NEI to be the 1- σ standard deviation of the calibrated continuum, we measured it for each instrument using a section of the continuum in each of the three atmospheric windows where planetary emission lines appeared to be absent and telluric absorption was known to be weak. These sections are indicated in Figs. 1–3.

Since the observations were obtained at disparate exposure times, resolutions, and samplings, transforming them to a common basis was necessary for each wavelength band in order to compare instrumental performance. Since the CGS4 slit and IFU slices both function as long slits sampling across Uranus’ disk, the disparate spatial resolution along these slits was neutralized by summing illuminated pixels along them (after medianing the IFU slices); so

for each instrument, a 1-D disk-averaged, and a 1-D diameter-averaged, flux spectrum was respectively generated for comparison.

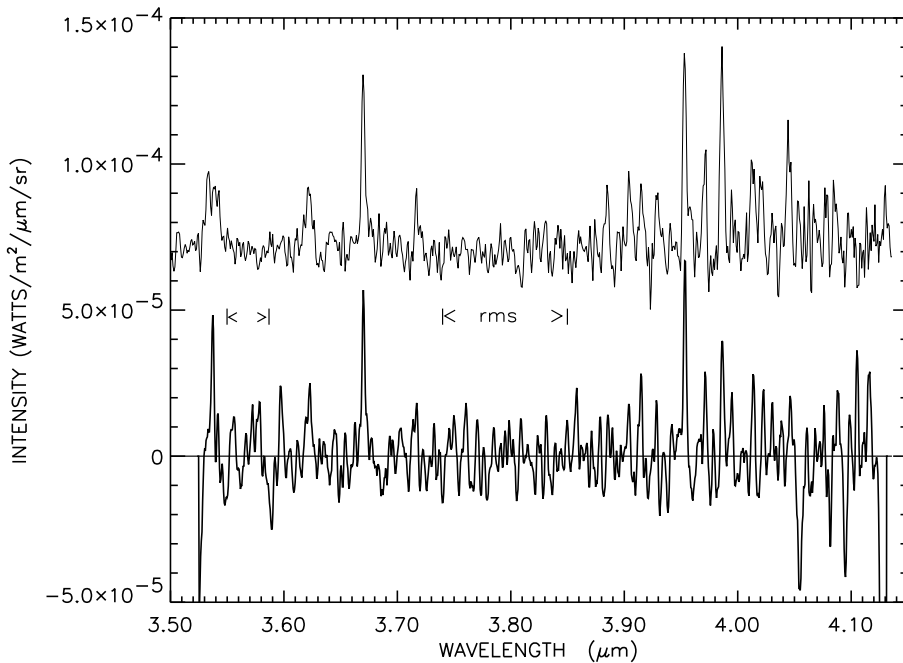


Fig. 3: Comparison of the extracted UIST/IFU spectrum of Uranus in the L'-band obtained on 23-24 Dec 2003 (heavy) (averaged over the portion of the disk visible in the IFU field) with a spectrum extracted from Uranus' equatorial diameter obtained with CGS4 on 19 Jun 2001 (light; offset $+7 \times 10^{-5}$). The IFU spectrum has been boxcar-smoothed over 4 pixels to match the instrumental spectral resolution of CGS4. Both spectra have been additionally smoothed by a Gaussian of FWHM=1.5 pixels. Emission from the fundamental band of H_3^+ is evident in the R branch on the left and the Q branch on the right. The ranges over which the standard deviation for the L'-band continuum was sampled are marked.

We adjusted the exposure times of CGS4 ($t_c \rightarrow t_{cs}$ in Table 2) to be consistent with the 2:1 pixel sampling per IFU slice (i.e., sampling the slit twice). Since the CGS4 spectra were effectively sampled 3:1 by shifting the spectrum by a third of a pixel sequentially between sub-exposures, the listed CGS4 exposure times were reduced 33%. Thus, a spectrum that is sampled 2:1 and observed in two-thirds the time has the same S/N per pixel as the one sampled 3:1.

Since CGS4 has the larger pixels and slit width, we used these modified CGS4 exposures, sampling, and original spectral and 1-D spatial resolutions as the common basis for comparing these instruments. The UIST/IFU spectra were, in effect, rebinned to match the CGS4 resolution elements, with two such IFU bins sampling each element. Since comparison of the spectral NEIs suffices, rather than the spectral features, we do not actually rebin the spectra but compensate either the exposure time at constant NEI or the NEI at constant exposure time to correspond to such rebinning. When the IFU exposure times are reduced proportionately by the aggregate pixels per bin, the resulting IFU spectrum has the same S/N or NEI per bin as the original had per pixel but now matches both the CGS4 spectral or spatial resolution and sampling. However, in matching the spatial resolution, we adjusted the NEI instead of the effective exposure time. For this purpose, the NEI per bin is assumed to scale as the square root of either the exposure time or the number of pixels or counts binned. This is the case for background-limited observations, and is expected to apply for the UIST/IFU exposures of Uranus (Detector exposure times of 2 min with HK, 1 min in

Short L, and 20 sec for Long L). In addition, Uranus’ HK continuum acts like an additional background when extracting the H₂ emission lines.

The spatial resolution element selected is thus the ~ 0.61 square pixel size of the CGS4 “long” camera, which matches the CGS4 slit width. This compares to the 0.24 width of the IFU image slices (spanned by two square pixels). The NEI values resulting from taking the standard deviation of the continuum regions marked in Figs. 1–3 for the extracted 1-D observed spectra (after Gaussian smoothing over 1.5 pixels) are tabulated in Table 2 as σ_c and σ_u for CGS4 and UIST/IFU, respectively. The NEI noise corresponding to a rebinning of the 0.24 wide IFU image slices to fill the 0.61 wide CGS4 slit, matching its spatial resolution with 2:1 sampling, was obtained by augmenting σ_u for the medianed 14 IFU slices by $\sqrt{14}/\sqrt{0.61/0.24} = 2.35$; this gave σ_{us} in Table 2.

Owing to grism ruling flaws, only the HK grism samples both the IFU spectral and spatial resolution elements twice, as designed. For the Short L and Long L spectra, 3.5 and 4.1 pixels are needed, respectively, to sample the spectral resolution element, although 2 pixels still span the width of each image slice. Comparison of R_c and R_u in Table 2 shows that the two instruments have nearly the same spectral resolution at HK and also at Short L; therefore, no resolution or sampling adjustment is needed for HK to match CGS4, and Short L needs only a 2:1 binning to approximately sample its effective spectral resolution element twice. This is achieved more accurately by reducing the Short L exposure time t_u by half the effective “IFU spectral sampling” (see Table 2), $3.5/2$, to yield t_{us} .

To compare Long L with CGS4, it was necessary to adjust both the mismatched spectral resolution and sampling. For IFU to match the CGS4 spectral resolution R_c spanned by 4.1 IFU pixels (see Table 2), the deconvolution of the grism-degraded Long L line spread function (LSF), having resolution R_u in Table 2, by one pixel (which yields a Gaussian of $\sigma=1.0$ pixel) must be convolved with a box of width 4.0 pixels. Therefore, IFU bins that are 2 pixels wide are needed for 2:1 sampling of the CGS4 resolution element; and boxcar smoothing of the IFU spectrum using a box of width equal to two such bins (i.e. 4 IFU pixels) is needed to match CGS4’s spectral resolution. This result is equivalent either to doubling the S/N, to boxcar smoothing over 4 pixels, or to reducing the effective exposure time of IFU by a factor of 4. The latter was done to yield t_{us} in Table 2 while the IFU spectrum in Fig. 3 was boxcar smoothed over 4 pixels. It is at this stage of analysis that the extracted UIST/IFU data are plotted in Figs. 1–3.

The mapping efficiency E of CGS4 relative to UIST/IFU can be expressed in terms of the relative time it takes the two instruments to obtain an equivalent map of Uranus; i.e., t_{us}/t_{map} . Here, t_{us} is the UIST/IFU exposure time that would result if its pixels were binned to sample the CGS4 resolution elements twice, and the exposure time were reduced to yield the same count or NEI per bin as originally per pixel. t_{map} is the time for CGS4 to map the the IFU field (equal to $6\times$ the CGS4 exposure time that gives the same S/N as an IFU binning that samples the CGS4 slit twice.) Thus, the formula for the efficiency of CGS4 relative to UIST/IFU for mapping Uranus is

$$E = \frac{1}{6} \frac{t_{us}}{t_{cs}} \left(\frac{\sigma_{us}}{\sigma_c} \right)^2 \quad (1)$$

where σ_c is the standard deviation of the CGS4 continuum, σ_{us} is the standard deviation of a sub-element of the IFU field equal to the width of the CGS4 spectrum over which IFU slices have been binned to match the CGS4 spectral resolution, and t_{cs} is the total exposure time for the CGS4 observation if it were sampled 2:1 instead of 3:1. Note that the optional 1.5 pixel Gaussian smoothing cancels out since it is applied to the spectra of both instruments. (The values of σ in Table 2 include this smoothing).

The values of E listed in Table 2 are greater than unity, varying from 1.4 to 2.5, showing that CGS4 is more efficient than UIST/IFU in mapping Uranus for all three windows tested. CGS4’s greater throughput and sensitivity evidently compensate for its restricted 2-D spectral coverage which, however, is large enough that comparatively few CGS4 observations

suffice to map the IFU field. In practice, the mapping of Uranus could be done by setting the CGS4 slit on the planet's central meridian and exposing in 1.5 hrs intervals over which the planet would rotate 30°. Six such exposures would then map a hemisphere at a S/N slightly better than shown in Figs. 1–3.

TABLE 2
Comparison of UIST/IFU vs CGS4 at K – L'

| Parameter (units) | 2.1 μm | 3.5 μm | 3.8 μm | Comment |
|--|----------------------|----------------------|-----------------------|---|
| R_c | 840 | 1400 | 1520 | Spectral resolution of CGS4 |
| CGS4 spectral sampling | 3 | 3 | 3 | Pixels per resolution element |
| t_c (min) | 70 | 78 | 78 | CGS4 exposure on 2001 June 19 |
| t_{cs} (min) | 47 | 52 | 52 | t_c adjusted to 2 pixels per slit ^a |
| σ_c ($Wm^{-2}\mu m^{-1}sr^{-1}$) | 1.8×10^{-7} | 3.0×10^{-6} | 4.8×10^{-6} | CGS4 rms noise in continuum ^b |
| R_u | 900 | 1380 | 2300 | Effective spectral resolution of IFU |
| IFU spectral sampling ^c | 2 | 3.5 | 4.1 | IFU pixels per CGS4 spectral res. el. |
| t_u (min) | 36 | 110 | 112 | UIST/IFU exposure times ^d |
| t_{us} (min) | 36 | 63 | 28 | t_u adjusted to 2 samples per res. el. |
| σ_u ($Wm^{-2}\mu m^{-1}sr^{-1}$) | 2.7×10^{-7} | 3.4×10^{-6} | 1.08×10^{-5} | IFU rms noise in continuum ^e |
| σ_{us} ($Wm^{-2}\mu m^{-1}sr^{-1}$) | 6.3×10^{-7} | 8.0×10^{-6} | 2.53×10^{-5} | IFU rms noise for CGS4 slit width |
| $r = \sigma_c / \sigma_{us}$ | 0.28 | 0.38 | 0.19 | CGS4/IFU rms noise ratio |
| $e_{eq} = r^2 t_{cs}$ (min) | 3.8 | 7.3 | 1.9 | IFU-equivalent CGS4 exposure |
| $t_{map} = 6 e_{eq}$ (min) | 23 | 44 | 11.2 | CGS4 time to map IFU field |
| $E = t_{us} / t_{map}$ | 1.6 | 1.43 | 2.5 | Relative efficiency of CGS4 to map the IFU field ^f |

The three wavelengths respectively lie within the K-, L-, and L'- bands. The comparison is made between the 1-D spectrum extracted along the CGS4 slit placed along Uranus' diameter vs that extracted along the IFU aperture slices and averaged across Uranus' disk. The noise is assumed to be background limited.

^ato give same number of counts per sample as before

^bafter 1.5 pixel Gaussian smoothing

^cnumber of IFU pixels spanning the CGS4 spectral resolution element (2 IFU pixels span the IFU slitlet)

^dwith the HK, Short L, & Long L grisms, respectively, on 2003 Sep10, Sep22, and Dec23-24.

^eafter 1.5 pixel Gaussian smoothing

^fvalue >1 implies CGS4 has the advantage

This CGS4 advantage may be less for brighter objects where sources of UIST/IFU fixed noise are not so important; e.g., readout noise. Also, shorter exposures will reduce the number of cosmic ray hits. Although taking the median of 14 IFU slices has eliminated most of these hits, their incidence nevertheless reduces the S/N ratio because fewer valid points are statistically compared in evaluating the median.

The feature around 3.53 μm that appears different in the two observations actually consists of both R(3) and R(2) transitions. The two R(3) transitions are nearly blended - para- H_3^+ R(3,2-) at 3.531 μm is very weak while the ortho- H_3^+ R(3,3-) at 3.534 μm is much stronger. There are then the two para- H_3^+ R(2) lines of nearly equal intensity, R(2,1-) at 3.538 μm and R(2,2-) at 3.542 μm . The relative intensities of these lines are sensitive to both

temperature and ortho-/para- H_3^+ ratio, with the R(3) to R(2) ratio increasing with increases in either parameter.

The R(3,3) line lies in the wing of a strong telluric CH_4 line and is Doppler shifted into it during the June 2001 observations, but not the UIST/IFU ones. It is thus particularly sensitive to how well matched the terrestrial atmospheric absorption is in the spectra of Uranus and the comparison star. This line is often weaker than it should be in planetary spectra, giving spuriously low temperatures on many occasions. Consequently, we discount its different appearance in our comparison of the performance of the two instruments.

In spite of the telluric CH_4 spectrum shown in Fig. 2, virtually all of the prominent features in Uranus' spectra shown here are due to H_3^+ rather than to noise. Of the prominent features in the UIST/IFU spectrum, only $3.391 \mu\text{m}$ appears to be solely noise. Some noise is evident where the spectrum dips negative (not counting the vignetting on the right) that may arise from miscancellation of the telluric CH_4 spectrum at these wavelengths during the flux calibration.

We do not expect much uncertainty in the IFU spectrum to arise from extracting a rectangular region of the IFU field even though Uranus' disk is circular. We have attempted to minimize the area of sky adjacent to Uranus in the selected rectangle so that its contribution to the noise in the 1-D extracted object - sky spectrum is minimal. The rms noise should be less sensitive to the area of Uranus extracted because the signal from the sky dominates Uranus' signal, especially in the L-L'-bands, and so contributes most of the statistical noise. However, IFU rows near the limb will cut a chord across Uranus' disk that includes a significant amount of dark sky so that the median of slices (columns) along that row will underestimate Uranus' intensity there. In general, the median does not work well to build up the S/N while excluding noise spikes when the source intensity varies from slice to slice by an amount that is greater than the noise. However, the effect of this on the total extracted spectrum is expected to be minor in the present case.

5 Conclusion

The results of Table 2 show conclusively that for all three telluric windows, CGS4 is more efficient than UIST/IFU for observing Uranus at moderate spectral resolution. A given S/N ratio is reached more quickly either by mapping Uranus' disk with multiple CGS4 observations or by setting the slit along the planet's CM and collecting observations while the planet rotates than by exposing once with UIST/IFU. Thus, the study of the spatial variation of K-L' band spectra over Uranus' disk is done more efficiently with CGS4 assuming its spatial resolution is adequate for the science.

This comparison between the two instruments is not comprehensive in that the shorter-wavelength windows and higher spectral resolution modes have not been included. IFU has been optimized for the HK grism, but only the K-band was compared. However, comparison of the relative sensitivity tables for these instruments on the UKIRT web site and the results for the windows compared here suggests that this conclusion is likely to hold for mapping Uranus at those wavelengths, as well.

More generally, when deciding in light of science objectives which of these instruments to use for observing a more general extended object, one must evaluate the specific target properties carefully against the opposing instrumental capabilities; i.e., spatial throughput vs sensitivity, to determine which would be more efficient. The important target properties are brightness, structure scale, size relative to the IFU field, whether rotation or time variability occurs, and the potential impact of cosmic ray hits from long exposures. Another consideration might be the nature of the spectrum; i.e., if both emission lines and a continuum are present, whether they are both resolved spatially. If accurate 2-D mapping or undistorted spectral imaging is required; or if spatial resolution greater than the CGS4 pixel size is required, then UIST/IFU would be the better instrument to use.

Acknowledgements: The United Kingdom Infrared Telescope is operated by the Joint Astronomy Centre on behalf of the U.K. Particle Physics and Astronomy Research Council. Some of the data reported here were obtained as part of the UKIRT Service Program. We thank the UKIRT staff for providing needed information on the UIST/IFU instrument, C. Davis for helpful comments, and especially thank Andy Adamson and Paul Hirst, who were particularly helpful with the service observing and data processing. This work was supported by NASA grants NAG5-10435 and NNG04G131G.

References

- Baines, K. H., Mickelson, M. E., Larson, L. E., & Ferguson, D. W. 1995. *Icarus*, 114, 328–340
- Fink, U., & Larson, H. P. 1979, *ApJ*, 233, 1021
- Lam, H. A., Miller, S., Joseph, R. D., Geballe, T. R., Trafton, L. M., Tennyson, J., & Ballester, G. E. 1997, *ApJ*, 474, L73
- Mountain, C.M., Robertson, D.J., Lee, T.J., & Wade, R. 1990, in *Instrumentation in Astronomy VII*, ed D.L. Crawford (*Proc. SPIE*, 1235), 25
Also see the CGS4 web page, www.jach.hawaii.edu/JACpublic/UKIRT/instruments/cgs4/cgs4.html
- Ramsay Howat, S.K., Atad, E. , Bennett, R., J., Bridger, A., Content, R., Ellis, M., Hastings, P., Strachan, M., Wall, R., & Wells, M. 1998, *SPIE Vol 3354*, p456
- Ramsay Howat, S. K., Ellis, M. A., Gostick, D. C., Hastings, P. R., Strachan, M., & Wells, M. 2000, *SPIE*, 4008, 1067
- Ramsay Howat, S., Todd, S., Leggett, S., Davis C., Strachan, M., Borrowman, A., Ellis, M., Elliot, J., Gostick D., Kackley, R., & Rippa, M. 2004, in *Proc SPIE*, 5492, in press
Also see the UIST web page, www.jach.hawaii.edu/JACpublic/UKIRT/instruments/uist/uist.html
- Todd, S.P, Wells, M., Ramsay Howat, S.K., & Hastings, P.R. 2003. “Cryogenic image slicing IFU for UKIRT: manufacture, alignment, laboratory testing, and data reduction”, in *Specialized Optical Developments in Astronomy*. Edited by Atad-Ettdedgui, E. & D’Odorico, S., *Proc. SPIE*, 4842, 151
- Trafton, L. M., Geballe, T. R., Miller, S., Tennyson, J., & Ballester, G. E. 1993, *ApJ*, 405, 761
- Trafton, L. M., Miller, S., Geballe, T. R., Tennyson, J., & Ballester, G. E. 1999, *ApJ*, 524, 1059